Int. J. Heat Mass Transfer. Vol. 30, No. 12, pp. 2641–2650, 1987
Printed in Great Britain

0017–9310/87 $3.00 + 0.00

Phase-change front prediction by measuring the wall temperature on which solidification occurs

MOON-HYUN CHUN,† HEON-OH CHOI,‡ HYUNG-GIL JUN† and YEON-SIK KIM†

† Department of Nuclear Engineering, Korea Advanced Institute of Science & Technology, P.O. Box 150, Cheongryang, Seoul, Korea, ‡ Korea Institute of Machinery & Metals, Changwon P.O. Box 41, Kyungsang-Namdo, Korea

(*Received* 20 *June* 1986 *and in final form* 11 *May* 1987)

Abstract—Experimental data for the liquid–solid interface position as a function of time and the wall temperature of the convectively cooled tube on which freezing occurs are obtained and compared with two theoretical predictions. These comparisons show that approximate values of the phase-change front can be estimated by measuring the surface temperature on which freezing occurs and using the data in a simple formula derived on the basis of a quasi-steady state assumption. For more accurate predictions, however, a numerical procedure based on the optimization technique is needed.

1. INTRODUCTION

THE PHENOMENA of liquid–solid phase change are of practical interest in a wide range of technical applications. For example, the melting and solidification processes have been extensively studied for the latent heat-of-fusion energy storage design [1–3], the assessment of molten fuel relocation following hypothetical core-disruptive accidents in liquid-metal-fast-breeder reactors [4–6], casting of metals [7] and desalination of water. The major characteristics of the melting and freezing problems include the movement of a phase boundary induced by the diffusion of energy or mass, and the nonlinearity associated with the moving phase boundary extremely complicates its analysis.

Those works reviewed by the authors could be classified into a few broad categories: (a) the exact closed form solutions [8, 9] which exist for some special cases where conduction is the sole mode of heat transfer, (b) approximate analytical and numerical solutions [6, 10] which take into consideration the effects of natural and/or forced convection, and (c) other parametric or ad hoc solutions [11, 12] that have been proposed for special applications.

The main objective of the present work is to examine the usefulness of two proposed methods for phase-change front predictions by application to a special case: one method requires a numerical procedure based on the optimization technique [13], whereas the other method uses a simple analytical model based on the quasi-steady state conduction approach. This paper presents the results of both experimental and theoretical studies on the phase-change front propagation when solidification of an initially stagnant superheated molten fluid occurs on the outside wall of a convectively cooled vertical tube. When the wall temperature of the cooled tube falls below the solidification temperature of the phase-change material (molten paraffin wax was used in the present work) freezing occurs along the outside wall of the cooled tube. During solidification, the phase-change front moves into the liquid and the shape of the freezing interface responds to the rate at which heat is being locally removed. The thickness of the frozen layer will grow until the amount of the local heat conducted through the frozen layer from the solidification interface to the convectively cooled tube wall becomes equal to the amount of local heat added to the interface by the superheated liquid surrounding the liquid–solid interface. A steady-state condition will be achieved if the net amount of energy being locally removed becomes zero at all locations along the liquid–solid interface.

To predict the transient position of the liquid–solid interface by either the optimization method [13] or the quasi-steady state conduction approach, one needs the temperature of the wall on which phase change is taking place. These techniques are suitable to obtain knowledge of the moving liquid–solid interface of the non-transparent phase-change material, in particular, where the photographical method cannot be used. It is also useful for the case of inward solidification of flowing fluid in a tube, where direct measurement of the liquid–solid interface is not possible, whereas the tube wall temperature measurement is relatively easy.

2. EXPERIMENTAL APPARATUS AND PROCEDURE

2.1. *Test apparatus*

To examine the applicability of both the simple analytical model developed in the present work and the minimization technique proposed earlier [13] to predict the phase-change front, one needs two sets of experimental data taken simultaneously. The first

NOMENCLATURE

D_e	equivalent diameter of the coolant channel	$T_b(t)$	bulk temperature of the coolant
g_m, g_n	shape function	T_f	fusion temperature
h	heat transfer coefficient for coolant flow	T_0	initial temperature of liquid and surface temperature of containment vessel
k	thermal conductivity of the solid phase	$T_w(r_i, t)$	temperature of the inside tube wall
k_b	thermal conductivity of the coolant water	$T_w(r_o, t)$	temperature of the outside tube wall
k_t	thermal conductivity of the tube	ΔT_i	inner temperature difference, $T_f - T_b$
L	unit length of the tube	ΔT_0	initial liquid superheat, $T_0 - T_f$
Pr	Prandtl number	U	overall heat transfer coefficient.
q	heat transfer rate	Greek symbols	
$q_c'(t)$	rate of heat flow per unit length of the tube	α	thermal diffusivity of the solid phase
q_l''	heat flux of the liquid phase at the liquid–solid interface	λ	latent heat of fusion
q_s''	heat flux of the solid phase at the liquid–solid interface	ρ	density of the solid phase.
Re	Reynolds number	Superscripts	
r_i	inner radius of the tube	k	time step
r_o	outer radius of the tube	$\hat{}$	quantities expressed by the finite element approximation
$r_s(t)$	transient position of the liquid–solid interface	*	shape function along the boundary.
t	time	Subscripts	
$T(r, t)$	temperature of the solid phase	l	liquid phase
		m, n	node indices
		s	solid phase.

data is the experimental values of solid–liquid interface position as a function of time, and the other is the wall temperature of the tube on which solidification is taking place. The former is needed to compare directly with predictions of both theories, while the latter is used as a boundary condition and as a known value, respectively, in the minimization formulation and in the analytical formula for the prediction of the phase-change front.

The experimental apparatus designed to obtain the above two sets of data was similar to the one used by Sparrow *et al.* [1]. A schematic diagram of the test cell is shown in Fig. 1. The major components of the test apparatus were: (a) a cooled cylindrical tube which was immersed in liquid paraffin during a data run so that the freezing could take place on the outside surface of the tube wall; (b) a cylindrical containment vessel situated in a temperature controlled water bath to contain a liquid paraffin (n-octadecane); (c) a constant temperature water bath and auxiliary systems for controlling the temperature of the cooled tube and temperature of the environment surrounding the phase-change medium.

The cooled cylindrical tube, which is concentric with the containment vessel, is a tube within a tube. The outer tube, which is 2.54 cm in diameter, is a thick-walled (0.2 cm thick) copper pipe. The inner tube, on the other hand, is of thin-walled copper (0.6 cm in diameter). As shown in Figs. 1 and 2, the coolant

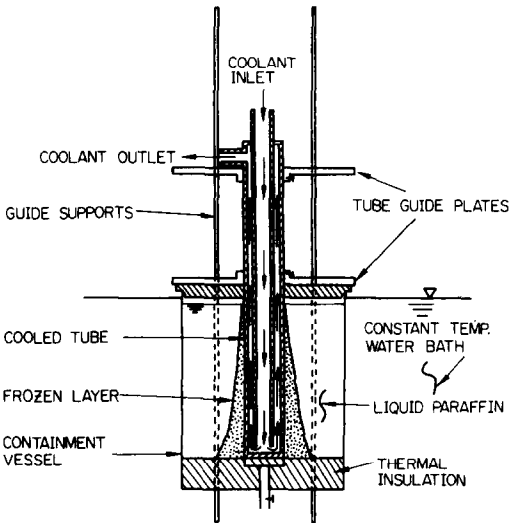

FIG. 1. Schematic diagram of test cell.

enters at the top of the inner tube and flows axially downward. At the bottom of the tube, the flow of coolant changes direction and passes upward through the annular space between the tubes, and finally flows out at the top. Dimensions are shown in Table 1.

The containment vessel, which is situated in a temperature controlled water bath, is 15 cm in diameter and 20 cm high. To isolate the lower regions of the

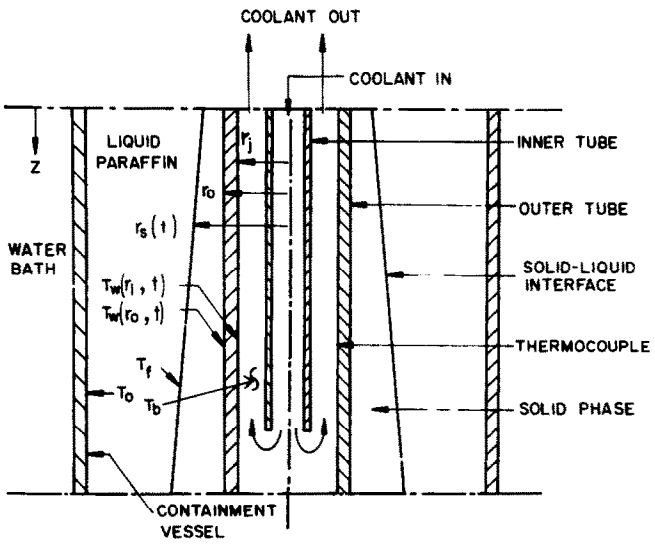

FIG. 2. Physical model for solidification on the outside wall of a convectively cooled tube.

Table 1. Test section geometry

	Inner tube	Outer tube	Containment vessel
i.d. (mm)	4.0	21.0	150.0
o.d. (mm)	6.0	25.4	155.0
Length (mm)	270.0	300.0	195.0
Material	copper	copper	stainless steel

frozen layer from thermal interactions with the lower wall of the containment vessel, a 5 cm thick compact-styrofoam insulation layer was attached to the bottom of the vessel. In addition, the insulation was covered with plastic-coated contact paper to ensure a smooth surface.

The constant temperature water bath was housed in an acrylic tank the dimensions of which were 50 cm deep, and 80 × 60 cm in horizontal cross-section. Temperature control and its uniformity were achieved by a thermostatically activated heating device which also served to circulate the water throughout the bath. As can be seen in Figs. 1 and 2, the constant temperature water bath enables the surface temperature of the vessel to be maintained at a constant value T_0.

To measure the wall temperature of the cooled tube on which solidification takes place, eight thermocouples were installed on the inside surface of the outer tube at axial positions located 1.5, 3.0, 4.5, 6.0, 7.5, 9.0, 10.5, and 12.0 cm, respectively from the lower end.

Controlled vertical positioning and axial movement of the cooled tube was performed by the support and guide structures shown at the top of Fig. 1. Four vertical supports, welded to the outer surface of the containment vessel, positioned a pair of guide plates through which the cooled tube is locked in place. Each guide plate is a 0.4 cm thick stainless-steel disc machined with a centre hole the diameter of which is slightly larger than that of the cooled tube. Each disc is equipped with a set screw.

The instrumentation for the experiments included analogue voltmeters, which could be read to 1 μV, for detecting the thermocouple outputs and associated recording equipment.

2.2. *Test parameters*

There are three temperature parameters that play a decisive role in the solidification process [1]: (a) the temperature $T_w(r_i, t)$ of the cooled tube on which the freezing occurs, (b) the solid–liquid interface temperature T_f (i.e. the temperature of the phase-change front), and (c) the initial temperature T_0 of the superheated liquid. Of these, the fusion temperature T_f is one of the physical properties of the phase-change material. The physical properties of the 97% pure n-octadecane paraffin used in the present work are given in Table 2. The other two temperatures constitute, along with the duration time of a data run, the main controllable test parameters. In the actual test, the inner surface temperature of the cooled tube $T_w(r_i, t)$ was controlled by controlling the coolant temperature T_b and the coolant flow rate.

In the present experiments, two levels of coolant temperature (i.e. $T_b = 19$ and 3°C, respectively) and two levels of initial molten fluid temperatures (i.e. $T_0 = 40$ and 34.5°C) were chosen as the main prescribable parameters. To specify test conditions, however, the above parameters will be reduced to a pair of temperature differences as follows:

$$\Delta T_i = T_f - T_b, \quad \Delta T_0 = T_0 - T_f. \qquad (1a, b)$$

Physically, ΔT_i is the temperature difference between the solidification temperature of the liquid paraffin and the coolant temperature, whereas ΔT_0 is the initial superheat of the liquid paraffin. These quantities will, in the subsequent discussion, be referred to respec-

Table 2. Physical properties of n-octadecane

	Solid	Liquid
Melting point (°C)	28	—
Heat of fusion (J kg^{-1})	243 000	—
Density (kg m^{-3})	814 (at 27°C)	774 (at 32°C)
Thermal conductivity (W m^{-1} K^{-1})	0.15 (at 28°C)	—
Specific heat (J kg^{-1} K^{-1})	2160	—
Viscosity (kg s^{-1} m^{-1})	—	0.00268 (at 40°C)

tively as the 'inner temperature difference' and 'liquid superheat'.

2.3. *Test procedure*

To obtain the experimental data of the phase-change front position vs time and the transient inner surface temperature of the outer tube $T_w(r_i, t)$, a succession of data runs of different duration times was performed for fixed values of ΔT_i and ΔT_0.

The constant temperature water bath and the containment vessel were first charged with water and molten paraffin wax. Prior to each data run, thermal equilibria were separately established in the liquid paraffin and in the cooled tube at the desired values of T_0 and T_w. During this preparatory period, the cylindrical tube was immersed in the liquid paraffin and maintained at the same temperature of the initial liquid paraffin (T_0) by passing the heated water through the tube. The wall temperature of the containment vessel was maintained at a uniform and constant temperature during each data run by the temperature controlled water bath.

When a thermal equilibrium between the liquid paraffin and the tube was reached, the data run was initiated by circulating the coolant water maintained at T_b through the tube, and a frozen layer was formed on the outside wall of the tube immediately. The inside wall temperature of the outer tube was measured as a function of time while the data run was allowed to proceed for a preselected duration. After duration of preselected times (i.e. at 1, 2, 3, 5, 10, 15, 20, 30, 45, and 60 min for each data run), the cooled tube, along with the attached frozen paraffin layer, was instantly raised vertically upward and pulled out of the containment vessel. Photographs of each frozen layer specimen along with a reference scale were taken, and measurements of the frozen layer thickness at various axial positions were made and recorded.

3. QUASI-STEADY STATE CONDUCTION APPROACH TO PREDICT PHASE-CHANGE FRONT

In an effort to demonstrate that the position–time history of a frozen front in a superheated melt can be inferred from measurements of the temperature history of the surface on which freezing takes place, a more basic analysis is first performed using a quasi-steady state conduction approach.

When solidification is taking place on the outside wall of a circular tube, while the inside wall of the tube is convectively cooled as shown in Fig. 2, the rate of heat transfer from the solidified layer to the outer tube wall in the steady state can be expressed as

$$q = 2\pi r L k \frac{dT}{dr} \quad \text{in } r_o \leqslant r \leqslant r_s. \tag{2}$$

On the other hand, the rate of heat transfer from the outer surface of the tube to the coolant is given by

$$q = 2\pi r_o L U [T_w(r_o, t) - T_b] \quad \text{for } r \leqslant r_o \tag{3}$$

where U is the overall heat transfer coefficient defined by

$$U = \frac{1}{\dfrac{1}{h} + \dfrac{r_i \ln (r_o/r_i)}{k_t}}. \tag{4}$$

Assuming a perfect thermal contact between the outside wall of the tube and the solidified layer, and equating equations (2) and (3) for a quasi-steady state the following equation can be obtained after rearranging:

$$dT = \frac{U r_o}{k} [T_w(r_o, t) - T_b] \frac{dr}{r}. \tag{5}$$

By integrating equation (5) from r_o to r_s and rearranging, the liquid–solid interface position as a function of time can be obtained as

$$r_s(t) = r_o \exp \left\{ \frac{k[T_f - T_w(r_o, t)]}{U r_o [T_w(r_o, t) - T_b]} \right\}. \tag{6}$$

The only unknown value in equation (6) is $T_w(r_o, t)$. In the present problem, $T_w(r_o, t)$ can be expressed in terms of $T_w(r_i, t)$, h, and T_b by the following relations:

$$T_w(r_o, t) - T_w(r_i, t) = \frac{q \ln (r_o/r_i)}{2\pi k_t L} \tag{7}$$

$$T_w(r_i, t) - T_b = \frac{q}{2\pi r_i L h}. \tag{8}$$

From equations (7) and (8) the following expression for $T_w(r_o, t)$ can be obtained for a quasi-steady state:

$$T_w(r_o, t) = \frac{r_i h}{k_t} [T_w(r_i, t) - T_b] \ln \left(\frac{r_o}{r_i} \right) + T_w(r_i, t). \tag{9}$$

Thus, the phase-change front position vs time $r_s(t)$

can be found from equation (6) by measuring the transient temperature of the tube wall, either $T_w(r_i, t)$ or $T_w(r_o, t)$, on which solidification is taking place. When equation (9) is used to obtain $T_w(r_o, t)$, the heat transfer coefficient h for coolant flow can be estimated from the existing correlations such as the Dittus–Boelter correlation [14] or the Sieder and Tate correlation [15].

4. MINIMIZATION FORMULATION TO PREDICT PHASE-CHANGE FRONT

4.1. *Mathematical formulation*

When a phase change occurs, the shape of the solid–liquid interface becomes a curved surface in general. However, if the surface is sufficiently smooth, it is possible to represent the phase-change process in one-dimensional form. Therefore, when solidification is taking place on the outside wall of a circular tube, while the inside wall of the tube is convectively cooled as shown in Fig. 2, the governing equation, initial and boundary conditions for the solid phase can be expressed as follows:

$$\frac{1}{\alpha}\frac{\partial T}{\partial t} - \frac{1}{r}\frac{\partial}{\partial r}\left(r\frac{\partial T}{\partial r}\right) = 0, \quad \text{in } r_s(t) > r > r_o, \quad t > 0 \tag{10}$$

$$T(r, t) = T_f, \quad \text{at } r = r_s(t), \quad t > 0 \tag{11}$$

$$r_o k\frac{\partial T}{\partial r} - r_i U(T - T_b) = 0, \quad \text{at } r = r_o, \quad t > 0 \tag{12}$$

$$r_s(t) = r_o, \quad \text{at } t = 0 \tag{13}$$

where $T(r, t)$ and $r_s(t)$ denote the temperature of the solid phase and the transient position of the solid–liquid interface, respectively.

Equation (11) expresses the fact that the temperature of the solid–liquid interface is at the fusion temperature T_f of the phase-change material. Equation (12) is a mixed boundary condition at the convectively cooled wall, where U is defined by equation (4). The initial condition, equation (13), denotes that no presolidified layer exists at the onset of solidification.

The transient position of the solid–liquid interface is determined by

$$\rho\lambda\frac{\partial r_s(t)}{\partial t} = -(q_s'' - q_l''), \quad \text{at } r = r_s(t) \tag{14}$$

where ρ, λ, q_s'' and q_l'' are the density, the latent heat of fusion, the heat flux of the solid phase and the heat flux of the liquid phase at the solid–liquid interface, respectively.

$r_s(t)$ is still unknown when both q_l'' and q_s'' are unknown. Note that q_l'' is difficult to obtain when convection is present in the liquid phase. Therefore, in order to trace the transient solid–liquid interface $r_s(t)$ in the present work, another boundary condition, equation (15), is used. That is, when the thermal conductivity of the tube wall is sufficiently large, the measured temperature of the inside wall of the tube, $T_w(r_i, t)$, is related to the outside wall temperature of the tube, $T_w(r_o, t)$, by the following equation:

$$T_w(r_o, t) = q_c'(t)\frac{\ln(r_o/r_i)}{2\pi k_t} + T_w(r_i, t) \tag{15}$$

where q_c' is the rate of heat flow per unit length of the tube by convection and is given by

$$q_c'(t) = 2\pi r_i h[T_w(r_i, t) - T_b(t)]. \tag{16}$$

Thus, equation (15) can be evaluated by experimentally measuring the inside wall temperature of the convectively cooled tube $T_w(r_i, t)$.

The outside wall temperature, $T_w(r_o, t)$, can also be approximated by the temperature of the solid phase at $r = r_o$, if perfect thermal contact between the outside wall of the tube and the solidified layer is assumed. Thus

$$T(r, t) = T_w(r_o, t), \quad \text{at } r = r_o. \tag{17}$$

This additional boundary condition, equation (17), in addition to equations (10)–(13), is employed to predict the transient position of the solid–liquid interface.

Since $r_s(t)$ is an unknown function, the above problem is difficult to solve in its original form. Therefore, the above problem is transformed into an equivalent minimization problem of finding the moving boundary $r_s(t)$ which minimizes the difference between the temperatures given by equation (17) and the temperature at $r = r_o$ calculated from the governing equation. Mathematically, the problem is to determine $r_s(t)$ which minimizes

$$\int_t |T_w(r_o, t) - T(r_o, t)|^2\, dt \tag{18}$$

and satisfies

$$\frac{1}{\alpha}\frac{\partial T}{\partial t} - \frac{1}{r}\frac{\partial}{\partial r}\left(r\frac{\partial T}{\partial r}\right) = 0, \quad \text{in } r_s(t) > r > r_o, \quad t > 0 \tag{19}$$

$$2\pi r_o k\frac{\partial T}{\partial r}(r_o, t) - q_c'(t) = 0, \quad T[r_s(t), t] = T_f \tag{20a, b}$$

$$r_s(0) = r_o. \tag{21}$$

It may be noted here that three major assumptions were made in the above mathematical formulation.

(1) Since the variation of the solidified-layer thickness as a function of time along the tube axis is sufficiently small compared to the radial growth rate in the present experiment, a one-dimensional approximation is made. Therefore, the governing equation for the solidified layer at each measuring point is given by equation (10).

(2) Since the thermal resistance of the tube wall is extremely small compared to the thermal resistance of the solidified layer of the phase-change material used in the present experiments (i.e. paraffin wax), a steady-state heat conduction in the tube wall is assumed.

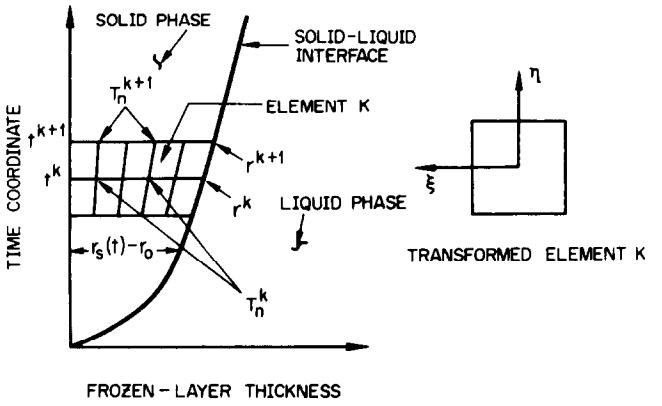

FIG. 3. Solution domain and transformed domain.

(3) The thermophysical properties of the frozen layer as well as the tube were assumed to be constant.

4.2. *Numerical procedure*

The proposed minimization problem is discretized using the finite element, suitable for numerical calculation. The solution domain of the state equation, equation (19), is continuously deforming with moving boundary $r_s(t)$, as shown in Fig. 3. Therefore, the space–time finite element is used to easily incorporate the continuously deforming domain. The isoparametric space–time finite element approximations for the temperature $T(r, t)$ and domain variables r and t can be written as

$$\hat{T}(r,t) = T_m g_m(\xi,\eta), \quad \hat{r} = r_m g_m(\xi,\eta), \quad \hat{t} = t_m g_m(\xi,\eta) \quad (22a\text{–}c)$$

where T_m, r_m and t_m are nodal values, and the summation convention is represented by the dummy index m. A linear interpolation function is used as the shape function as shown in Fig. 3.

To have only one design variable in the discretized form and to increase the efficiency of calculation, one discretization in the time coordinate is made. The Galerkin finite element procedure is applied to the state equation, equation (19), with one discretization in the time coordinate. Thus

$$2\pi \int_{t^k}^{t^{k+1}} \int_{r_o}^{r_s(t)} g_m \left[\frac{1}{\alpha}\frac{\partial \hat{T}}{\partial t} - \frac{1}{r}\frac{\partial}{\partial r}\left(r \frac{\partial \hat{T}}{\partial r} \right) \right] r \, dr \, dt = 0. \quad (23)$$

Using the Green–Gauss theorem on the transient term as well as on the diffusion term and then applying the initial and boundary condition, equation (23) becomes

$$2\pi \int_{t^k}^{t^{k+1}} \int_{r_o}^{r_s(t)} \left(-\frac{1}{\alpha}\frac{\partial g_m}{\partial t} g_n + \frac{\partial g_m}{\partial r}\frac{\partial g_n}{\partial r} \right) r \, dr \, dt T_n + 2\pi \int_{r_o}^{r_s(t^{k+1})} \frac{1}{\alpha} g_m^* g_n^* r \, dr \, T_n - \int_{t^k}^{t^{k+1}} \frac{1}{k} g_m^* q_c'(t) \, dt = 0 \quad (24)$$

where g_m^* and g_n^* in the second term and g_m^* in the third term represent the shape function defined on the boundary of the solution domain, and $dr\, dt = J\, d\xi\, d\eta$ where J is the Jacobian defined by $\partial(r, t)/\partial(\xi, \eta)$.

The design variable $r_s(t)$ is reduced to $r_s(t^{k+1})$ (see Fig. 3) and the objective function, equation (18), is reduced to

$$|T_w(r_o, t^{k+1}) - T(r_o, t^{k+1})|^2. \quad (25)$$

Therefore, the discretized version of the minimization problem using the space–time finite element with one discretization in the time coordinate is reduced to a problem of finding $r_s(t^{k+1})$ which minimizes the objective function, equation (25), and satisfies the state equation, equation (24).

In this approach, the results of the previous time step are used as the initial condition of the present step.

Since the number of design variables is reduced to one in the formulation of the minimization problem in the numerical procedure, the Fibonacci search technique [16] is used to find $r_s(t^{k+1})$, simultaneously solving the state equation, equation (24).

5. EXPERIMENTAL RESULTS AND COMPARISON WITH MODEL

To test the applicability of the two theoretical approaches by comparing with experimental data and to examine the effects of the two temperature parameters (ΔT_0 and ΔT_i) on the phase-change front velocity, four data runs were made at two levels of the inner temperature difference and at two different liquid superheats: the first two data runs were made at two levels of initial liquid superheat (i.e. $\Delta T_0 = 12$ and 6.5°C, respectively) while ΔT_i is maintained constant ($\Delta T_i = 9$°C). For the other two data runs, ΔT_i was raised and fixed at 25°C while using the two levels of initial liquid superheat (i.e. $\Delta T_0 = 12$ and 6.5°C).

For each data run, ten different run times were used

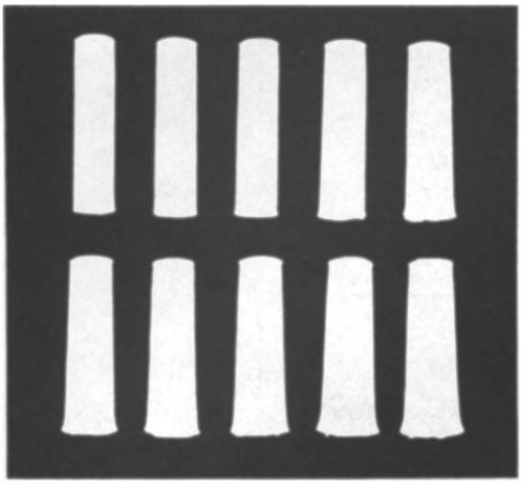

FIG. 4. Typical solidified layer growth pattern in a superheated liquid ($\Delta T_i = 25°C$, $\Delta T_0 = 6.5°C$); run times (top left to bottom right): 1, 2, 3, 5, 10, 15, 20, 30, 45 and 60 min.

varying from 1 to 60 min, and photographs of each frozen layer specimen were taken to obtain a quantitative data on the timewise growth of the frozen layer. A typical solidified-layer growth pattern in a superheated liquid is displayed photographically in Fig. 4. The test conditions for this case were $\Delta T_i = 25°C$ and $\Delta T_0 = 6.5°C$, respectively. As reported by previous workers on 'freezing controlled by natural convection' [1], freezing in the presence of superheating yields a gently contoured surface, with the thickness of the frozen layer increasing from top to bottom.

5.1. *Effect of cooling rate*

According to equation (16) an increase of ΔT_i by decreasing T_b in equation (1a), the cooling rate of the tube $q_c'(t)$ will be increased. During the transient period, the necessary condition for solidification is $q_s'' > q_l''$ in equation (14). The rate of solidification is determined by the quantity given by the right-hand side of equation (14). Since an increase of $q_c'(t)$ is equivalent to increasing q_s'', the thickness of the frozen layer increases when ΔT_i is increased at a fixed ΔT_0. This deduced result can be confirmed by comparing the two sets of experimental data shown in Fig. 5 ($\Delta T_i = 9°C$, $\Delta T_0 = 12°C$) and Fig. 7 ($\Delta T_i = 25°C$, $\Delta T_0 = 12°C$) or Fig. 6 ($\Delta T_i = 9°C$, $\Delta T_0 = 6.5°C$) and Fig. 8 ($\Delta T_i = 25°C$, $\Delta T_0 = 6.5°C$). For example, the final thickness of the frozen layer in Fig. 5 is 1.1 mm (curve B), whereas the final thickness in Fig. 7 is 5.4 mm (curve B) for the same duration time of 60 min.

5.2. *Effect of initial molten fluid superheat*

According to equation (1b), ΔT_0 can be varied by varying the initial temperature of the molten paraffin wax T_0. For the solidification of the molten fluid, the latent heat as well as the sensible heat of the molten fluid must be removed. When ΔT_0 is decreased by decreasing the initial temperature of the molten fluid T_0, the amount of sensible heat to be removed for solidification becomes smaller. Thus, a decrease in ΔT_0 at a fixed ΔT_i will bring about an increase in the final thickness of the frozen layer and a shorter freezing time. Comparison of the solidified layer thickness vs time curves shown in Figs. 5 and 6 as well as the curves shown in Figs. 7 and 8 confirms the above physical deductions. For example, the final thickness of the frozen layer in Fig. 7 is about 5.5 mm (curve B), whereas curve B of Fig. 8 is about 6.8 mm for the same duration time of 60 min.

5.3. *Comparison between theory and experimental data*

It may be noted here that one needs the values of h in equation (4) for theoretical predictions of the phase-change front. The heat transfer coefficient h, in the present work, was estimated from the Dittus–Boelter correlation [14]

$$h = 0.023\left(\frac{k_b}{D_e}\right)(Re)^{0.8}(Pr)^{0.4}. \tag{26}$$

The two h values obtained from equation (26), using the proper test parameters and thermo-physical properties of water for $T_b = 19°C$ ($\Delta T_i = 9°C$) and $T_b = 3°C$ ($\Delta T_i = 25°C$), were 2521 and 3151 W m^{-2} °C^{-1}, respectively.

Figures 5 and 6 show the results for smaller ΔT_i (i.e. 9°C), whereas Figs. 7 and 8 show the results for larger ΔT_i (i.e. 25°C). From the results shown in these figures the following observations can be made.

(1) Figures 5 and 6 show that the measured wall temperature of the outer tube $T_w(r_i, t)$, while the solidification process continued on its outer surface for times greater than 1 min, remained at a fairly constant value (about 20°C) substantially below the freezing temperature of the liquid paraffin ($T_f = 28°C$). Figures 7 and 8, on the other hand, show that $T_w(r_i, t)$ varied from 5.1°C (at $t = 1$ min for curves A) to 3.9°C (at $t = 60$ min for curves A) and the algebraic mean values of $T_w(r_i, t)$ for Figs. 7 and 8 were 15.5°C lower than that for Figs. 5 and 6 giving a larger solidification rate.

(2) When ΔT_i is relatively smaller (i.e. 9°C as in Figs. 5 and 6) the difference between the two wall temperatures measured at A and B is very small, and the difference in the solidification rates between the two points is also very small. However, when ΔT_i is relatively large (i.e. 25°C as in Figs. 7 and 8), the difference in the two $T_w(r_i, t)$'s measured at A and B is slightly larger than the previous case, and the phase-change front velocity at the lower axial position B, where the tube wall temperature is lower, is substantially larger than that at A.

(3) The agreement between the two theoretical curves of the frozen layer thickness vs time and the experimental data is fairly close and consistent when ΔT_i is relatively small as can be seen in Figs. 5 and 6. For larger ΔT_i (as in Figs. 7 and 8), on the other hand, the quasi-steady state approach, equation (6), gives

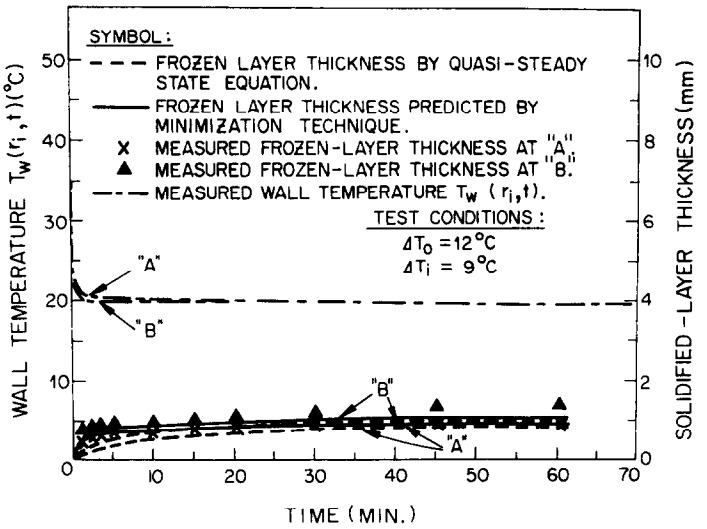

FIG. 5. Comparison between experimental results and two theoretical predictions for solidified layer thickness vs time at two axial positions on the tube (A = 9 and B = 3 cm from the bottom).

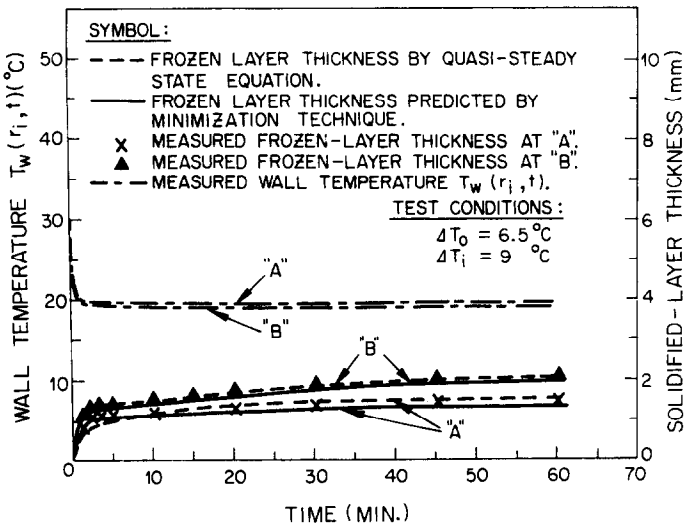

FIG. 6. Comparison between experimental results and two theoretical predictions for solidified layer thickness vs time at two axial positions on the tube (A = 9 and B = 3 cm from the bottom).

smaller solidification rates than the experimental data, whereas the agreement between the solidification rates obtained by the numerical procedure based on the optimization technique and the experimental data is still fairly good and consistent. This indicates that the quasi-steady state approach is not as good as the optimization technique when the solidification rate is large due to large ΔT_i.

6. CONCLUSION

Experiments on the solidification of an initially stagnant superheated liquid on the outside wall of a convectively cooled vertical tube were carried out to obtain the experimental data of (a) the phase-change front position vs time and (b) the transient temperature of the tube wall on which solidification is taking place. A comparison of the experimental data with predictions of two different approaches indicates that when the solidification rate is small due to small ΔT_i the phase-change front can be estimated by measuring the surface temperature on which freezing occurs and using the data in any one of the two approaches presented here; however, when the solidification rate is large due to the large temperature difference between the solidification temperature of the liquid and the coolant temperature, ΔT_i, the deviation between the experimental data and the predictions of the simple formula (equation (6)) based on the quasi-steady state approach becomes large. Therefore, when the solidification rate is large the optimization technique may be used for the more

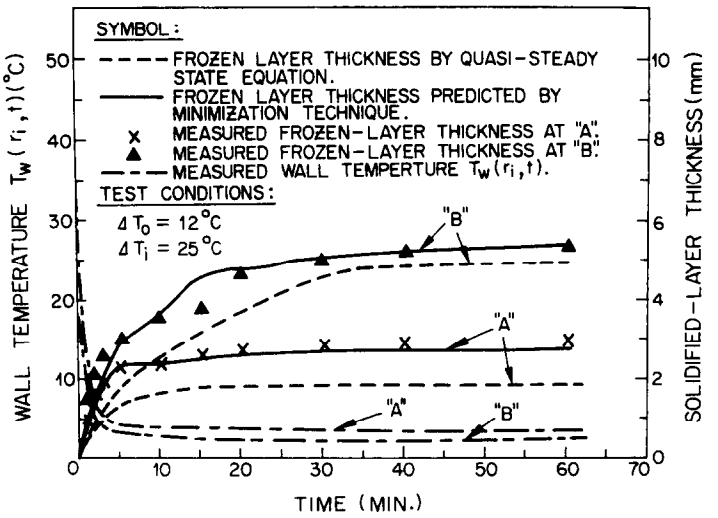

FIG. 7. Comparison between experimental results and two theoretical predictions for solidified layer thickness vs time at two axial positions on the tube (A = 9 and B = 3 cm from the bottom).

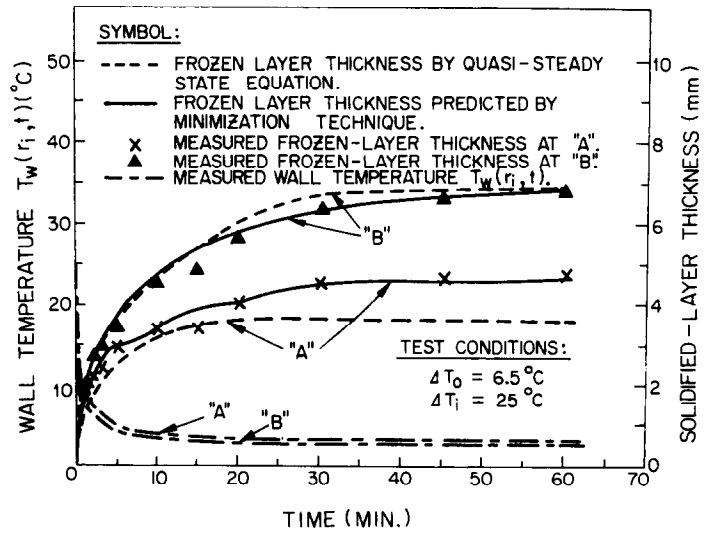

FIG. 8. Comparison between experimental results and two theoretical predictions for solidified layer thickness vs time at two axial positions on the tube (A = 9 and B = 3 cm from the bottom).

accurate estimation at the expense of longer computing times. In summary, the two approaches presented here have a great potential in the predictions of the phase-change front. These methods are suitable, in particular, to obtain the knowledge of the transient phase-change interface where direct measurements or photographical recordings are not possible, whereas the measurement of the convectively cooled surface temperature is relatively easy. However, these methods are useful only in those situations where one is sure that good thermal contact is maintained between the wall and the freezing layer.

REFERENCES

1. E. M. Sparrow, J. W. Ramsey and R. G. Kemink, Freezing controlled by natural convection, *J. Heat Transfer* **101**, 578–584 (1979).
2. E. M. Sparrow and C. F. Hsu, Analysis of two-dimensional freezing on the outside of a coolant-carrying tube, *Int. J. Heat Mass Transfer* **24**, 1345–1357 (1981).
3. C. J. Ho and R. Viskanta, Inward solid-liquid phase-change heat transfer in a rectangular cavity with conducting vertical walls, *Int. J. Heat Mass Transfer* **27**, 1055–1065 (1984).
4. M. Epstein, L. J. Stachyra and G. A. Lambert, Transient solidification in flow into a rod bundle, *J. Heat Transfer* **102**, 330–334 (1980).
5. M. H. Chun, R. D. Gasser, M. S. Kazimi, T. Ginsberg and O. C. Jones, Jr., Dynamics of solidification of flowing fluids with applications to LMFBR post-accident fuel relocation, *Proc. Int. Mtg. on Fast Reactor Safety and Related Physics*, Vol. IV, pp. 1808–1818 (1976).
6. M. H. Chun and S. W. Chung, Analysis of forced convection melting in a vertical channel for applications to

LMFBR post-accident fuel relocation, *Proc. 3rd Int. Topical Mtg. on Reactor Thermal Hydraulics*, pp. 19.D-1–19.D-7 (1985).
7. R. Siegel, Analysis of solidification interface shape resulting from applied sinusoidal heating, *J. Heat Transfer* **104,** 13–18 (1982).
8. J. Stefan, Uber die Theorie der Eisbildung, isbesondere uber dic Eisbildung in Polarmcere, *Ann. Phys. Chem.* **42,** 269 (1891).
9. H. S. Carslaw and J. C. Jaeger, *Conduction of Heat in Solids*, 2nd Edn, pp. 283–296. Oxford University Press, New York (1959).
10. E. M. Sparrow, S. V. Patankar and S. Ramadhyani, Analysis of melting in the presence of natural convection in the melt region, *J. Heat Transfer* **99,** 520–526 (1977).
11. R. S. Gupta and A. Kumar, Treatment of multi-dimensional moving boundary problems by coordinate transformation, *Int. J. Heat Mass Transfer* **28,** 1355–1366 (1985).
12. N. Shamsundar and R. Srinivansan, A new similarity method for analysis of multi-dimensional solidification, *J. Heat Transfer* **101,** 585–591 (1979).
13. H. O. Choi and M. H. Chun, Prediction of the phase change front using the optimization technique, *Int. Commun. Heat Mass Transfer* **12,** 647–656 (1985).
14. F. W. Dittus and L. M. K. Boelter, *Univ. Calif. Publs Engng* **2,** 443 (1930).
15. E. N. Sieder and G. E. Tate, Heat transfer and pressure drop of liquids in tubes, *Ind. Engng Chem.* **28,** 1429–1435 (1936).
16. D. G. Luenberger, *Introduction to Linear and Nonlinear Programming*, p. 134. Addison-Wesley, Reading, Massachusetts (1973).

PREDICTION DU FRONT DE CHANGEMENT DE PHASE A PARTIR DE LA MESURE DE LA TEMPERATURE DE LA PAROI SUR LAQUELLE SE FAIT LA SOLIDIFICATION

Résumé—On compare deux prédictions théoriques avec les données expérimentales sur la position, en fonction du temps et de la température pariétale, d'un interface liquide–solide pour un tube refroidi sur lequel se produit la solidification. Ces comparaisons montrent que les valeurs approchées du front de changement de phase peuvent être estimées en mesurant la température de la surface sur laquelle se produit la solidification et en utilisant les données d'une formule simple dérivée d'une hypothèse d'état stationnaire. Pour des prédictions plus précises, une procédure numérique basée sur une technique d'optimisation est nécessaire.

BESTIMMUNG DER PHASENÄNDERUNGSFRONT DURCH MESSUNG DER WANDTEMPERATUR BEI DER ERSTARRUNG

Zusammenfassung—Es werden experimentelle Daten für die flüssigfest Phasengrenze als Funktion der Zeit und der Wandtemperatur eines Rohres vorgestellt, an dem aufgrund konvektiver Kühlung Gefrieren stattfindet. Die Meßwerte werden mit zwei theoretischen Modellen verglichen. Dieser Vergleich zeigt, daß die ungefähre Lage der Phasenänderungsfront durch Messung der Temperatur an der Oberfläche, an welcher das Gefrieren stattfindet, und durch Andwendung einer einfachen Gleichung, die vom quasistationären Zustand abgeleitet wurde, bestimmt werden können. Für eine genauere Bestimmung ist jedoch ein numerisches Verfahren auf der Grundlage der Optimierungstechnik erforderlich.

ОПРЕДЕЛЕНИЕ ПОЛОЖЕНИЯ ФРОНТА ФАЗОВЫХ ПРЕВРАЩЕНИЙ ПУТЕМ ИЗМЕРЕНИЯ ТЕМПЕРАТУРЫ СТЕНКИ, НА КОТОРОЙ ПРОИСХОДИТ ЗАТВЕРДЕВАНИЕ

Аннотация—Получены экспериментальные данные для зависимости положения границы раздела фаз жидкость–твердое тело от времени и температуры стенки конвективно охлаждаемой трубы, на которой происходит затвердевание, и проведено их сравнение с результатами двух теоретических расчетов. Сравнение показало, что приближенные значения положения фронта фазовых превращений можно получить, измеряя температуру упомянутой поверхности и подставляя ее в простую формулу, полученную на основе квазистационарного приближения. Однако, для получения точных результатов требуется использование методов численной оптимизации.